

# Physicochemical and Spectroscopic Characterization of Biofield Treated Butylated Hydroxytoluene

Trivedi MK<sup>1</sup>, Branton A<sup>1</sup>, Trivedi D<sup>1</sup>, Nayak G<sup>1</sup>, Singh R<sup>2</sup> and Jana S<sup>2\*</sup>

<sup>1</sup>Trivedi Global Inc., 10624 S Eastern Avenue Suite A-969, Henderson, NV 89052, USA

<sup>2</sup>Trivedi Science Research Laboratory Pvt. Ltd., Hall-A, Chinar Mega Mall, Chinar Fortune City, Hoshangabad Rd., Bhopal-462026, Madhya Pradesh, India

## Abstract

The antioxidants play an important role in the preservation of foods and the management of oxidative stress related diseases by acting on reactive oxygen species and free radicals. However, their use in high temperature processed food and pharmaceuticals are limited due to its low thermal stability. The objective of the study was to use the biofield energy treatment on butylated hydroxytoluene (BHT) i.e. antioxidant and analyse its impact on the physical, thermal, and spectral properties of BHT. For the study, the sample was divided into two groups and termed as control and treated. The treated group was subjected to biofield energy treatment. The characterization of treated sample was done using X-ray diffraction (XRD), differential scanning calorimetry (DSC), thermogravimetric analysis (TGA), Fourier transform infrared (FT-IR) and UV-visible (UV-Vis) spectroscopy. The XRD results showed the alteration in lattice parameters, unit cell volume, and molecular weight along with 14.8% reduction in the crystallite size of treated sample as compared to the control. The DSC analysis showed an increase in the latent heat of fusion from 75.94 J/g (control) to 96.23 J/g in the treated BHT sample. The TGA analysis showed an increase in onset temperature of decomposition (130°C→136°C) and maximum thermal decomposition temperature (152.39°C→158.42°C) in the treated sample as compared to the control. Besides, the FT-IR analysis reported the shifting of aromatic C-H stretching peak towards higher frequency (3068→3150 cm<sup>-1</sup>) and C=C stretching towards lower frequency (1603→1575 cm<sup>-1</sup>) as compared to the control sample. Moreover, the UV spectrum also revealed the shifting of the peak at  $\lambda_{max}$  247 nm (control) to 223 nm in the treated sample. The overall results showed the impact of biofield energy treatment on physical, thermal and spectral properties of BHT sample.

**Keywords:** Biofield energy treatment; Butylated hydroxytoluene; Reactive oxygen species; Complementary and alternative medicine; Thermogravimetric analysis

## Introduction

In recent years, the studies on reactive oxygen species (ROS), free radicals and antioxidants are generating medical revolution by promising a good health and disease management [1]. The free radicals and ROS can be developed inside the human body either through the normal metabolic process or external sources such as pollutants, industrial chemicals, and cigarette smoking, etc. [2]. An antioxidant is a molecule that neutralises these free radicals by donating an electron to them. They prevent the oxidative reaction that is responsible for various chronic degenerative diseases viz. cancer, cardiovascular and neurodegenerative disorders, etc. [3]. Besides, in the pharmaceutical industry, the safety, efficacy and stability of drug formulations are affected by various physical factors like humidity, heat, and light [4]. These factors are responsible for several chemical reactions that cause instability such as oxidation, decarboxylation, hydrolysis, and photolysis, etc. [5]. The antioxidants are such excipients that can enhance the shelf-life of the drug by reducing the problem due to oxidation reactions. Butylated hydroxytoluene (BHT) is a monohydric phenol derivative (Figure 1) that provides electrons or protons labile to free radicals and interrupts the chain reaction thereby exerting its antioxidant action [6]. It is used as antioxidant in foods containing fats and oils as they are very susceptible to rancidity and oxidation that destroy the soluble vitamins and fatty acids. BHT prevents this rancidification by terminating the free radical chain reactions [7,8]. It helps in food preservation by preventing any change in flavour and slowing the rancidity and discoloration processes [9]. Moreover, it is also added in personal care products to prevent oxidative rancidity thereby disagreeable smell [10]. The antioxidants are also added in several manufacturing processes to protect the raw material and end product from deleterious effects of high temperature and pressure [11].

In food preservation process, the thermal stability of antioxidant is very crucial. Several edible oils are used at higher temperature; hence thermal stability of antioxidant is necessary to preserve the unsaturated fatty acid from degradation [12]. Despite several uses, BHT is sensitive to heat, light and humidity and is also known to possess some toxic and flammable properties hence need special precautions during storage, handling, and transportation [13,14]. Moreover, BHT is reported to decompose at low temperature due to which it offers very less protection to heated vegetable oils [15]. Thus, it is important to search

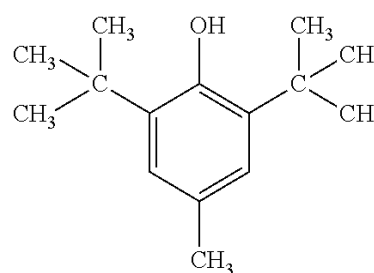


Figure 1: Chemical structure of butylated hydroxytoluene.

**\*Corresponding author:** Jana S, Trivedi Science Research Laboratory Pvt. Ltd., Hall-A, Chinar Mega Mall, Chinar Fortune City, Hoshangabad Rd., Bhopal- 462026, Madhya Pradesh, India, Tel: +91-755-6660006; E-mail: [publication@trivedieffect.com](mailto:publication@trivedieffect.com)

**Received** September 23, 2015; **Accepted** September 29, 2015; **Published** October 09, 2015

**Citation:** Trivedi MK, Branton A, Trivedi D, Nayak G, Singh R, et al. (2015) Physicochemical and Spectroscopic Characterization of Biofield Treated Butylated Hydroxytoluene. J Food Ind Microbiol 1: 101.

**Copyright:** © 2015 Trivedi MK, et al. This is an open-access article distributed under the terms of the Creative Commons Attribution License, which permits unrestricted use, distribution, and reproduction in any medium, provided the original author and source are credited.

some alternate strategies, which could improve the stability of BHT by altering their physical, thermal or structural and bonding properties.

Nowadays, biofield energy treatment is known to alter physicochemical properties of various organic and metallic compounds [16-19]. The biofield energy healing therapies are considered as complementary and alternative medicine (CAM) by National Center for Complementary and Alternative Medicine (NCCAM)/National Institute of Health (NIH) and are based on alteration in putative energy fields and consciousness [20,21]. The biofield energy is related to the energy associated with the human body that depends upon the physiological and mental health of the human. This energy can be exchanged with the environment through natural exchange process [22]. A human has the ability to harness the energy from environment or universe and can transmit in any living or non-living object(s) around the Universe. The objects always receive the energy and responding in a useful way, this process is known as biofield energy treatment. Moreover, the biofield therapies are reported for the reduction in pain, anxiety and tension [23]. Mr. Trivedi is well known to possess the unique biofield energy treatment (The Trivedi Effect) which is reported to alter the properties such as growth and yield of plants in the field of agriculture [24,25]. The effect was also reported on phenotypic characters of microorganisms in the field of microbiology [26,27]. Hence, the present study was designed to analyse the impact of biofield energy treatment on various physicochemical properties of BHT using XRD, DSC, TGA/DTG, FT-IR and UV-Vis spectroscopic techniques.

## Materials and Methods

### Material procurement

Butylated hydroxytoluene (BHT) was procured from S D Fine Chemicals Pvt. Ltd., India. After procurement, the BHT sample was divided into two parts; coded as control and treated, and stored as per manufacturer's guidelines.

### Treatment modality

The treated part was subjected to Mr. Trivedi's biofield energy treatment. For this, the treated sample was handed over to Mr. Trivedi in sealed pack for biofield energy treatment under standard laboratory conditions. Mr. Trivedi provided the treatment to the treated group through his energy transmission process. The biofield treated sample was returned in the same sealed condition for further characterization using XRD, DSC, TGA, FT-IR and UV-Vis spectroscopic techniques.

### X-ray diffraction (XRD) study

X-ray powder diffractogram of control and treated samples were obtained on Phillips, Holland PW 1710 X-ray diffractometer system. The X-ray generator was equipped with a copper anode with nickel filter operating at 35 kV and 20 mA. The wavelength of radiation used by the XRD system was 1.54056 Å. The data were collected from the  $2\theta$  range of  $10^\circ$ - $99.99^\circ$  with a step size of  $0.02^\circ$  and a counting time of 0.5 seconds per step.

The crystallite (G) was calculated from the Scherrer equation with the method based on the width of the diffraction patterns obtained in the X-ray reflected crystalline region.

$$G = k\lambda / (b \cos\theta)$$

Where, k is the equipment constant (0.94),  $\lambda$  is the X-ray wavelength (0.154 nm), b in radians is the full-width at half of the peak and  $\theta$  the

corresponding Bragg angle. Other parameters *viz.* lattice parameter and unit cell volume, were calculated using PowderX software. Further, these parameters were used to calculate the molecular weight and density of the control and treated sample.

Percent change in crystallite size was calculated using the following equation:

$$\text{Percent change in crystallite size} = [(G_t - G_c) / G_c] \times 100$$

Here,  $G_c$  and  $G_t$  denotes the crystallite size of control and treated powder samples, respectively. Similarly the percent change in lattice parameter, unit cell volume, molecular weight, and density was calculated to analyse the impact of biofield treatment on crystal parameters of treated sample as compared to the control.

The molecular weight of atom was calculated using following equation:

Molecular weight = number of electrons  $\times$  weight of an electron + number of neutrons  $\times$  weight of a neutron + number of protons  $\times$  weight of a proton.

The weight of all atoms in a molecule was multiplied by the Avogadro number ( $6.023 \times 10^{23}$ ) to obtain the molecular weight in g/Mol.

### Differential scanning calorimetry (DSC) study

DSC analysis of control and treated sample was carried out using Perkin Elmer/Pyris-1. Each sample was accurately weighed and hermetically sealed in aluminium pans and heated at a rate of  $10^\circ\text{C}/\text{min}$  under air atmosphere (5 mL/min). The thermogram was collected over the temperature range of  $50^\circ\text{C}$  to  $250^\circ\text{C}$ . An empty pan sealed with cover pan was used as a reference sample. From DCS curve, the melting temperature and latent heat of fusion were obtained.

The percent change in latent heat of fusion was obtained using following equations to observe the difference in thermal properties of treated BHT sample as compared to the control:

$$\% \text{ change in latent heat of fusion} = \frac{[\Delta H_{\text{Treated}} - \Delta H_{\text{Control}}]}{\Delta H_{\text{Control}}} \times 100$$

Where,  $\Delta H_{\text{Control}}$  and  $\Delta H_{\text{Treated}}$  denotes the latent heat of fusion of control and treated samples, respectively.

### Thermogravimetric analysis/Derivative Thermogravimetry (TGA/DTG)

The effect of temperature on the stability of the control and treated sample of BHT was analysed using Mettler Toledo simultaneous thermogravimetric analyser (TGA/DTG). The samples were heated from room temperature to  $350^\circ\text{C}$  with a heating rate of  $5^\circ\text{C}/\text{min}$  under air atmosphere. From TGA/DTG curve, the onset temperature  $T_{\text{onset}}$  (temperature at which sample start losing weight) and  $T_{\text{max}}$  (maximum thermal degradation temperature) were recorded.

### Fourier transform-infrared (FT-IR) spectroscopic characterization

For FT-IR characterization, the treated sample was divided into two groups named T1 and T2. The samples were crushed into fine powder for analysis. The powdered sample was mixed in spectroscopic grade KBr in an agate mortar and pressed into pellets with a hydraulic press. FT-IR spectra were recorded on Shimadzu's Fourier transform infrared spectrometer (Japan). FT-IR spectra are generated by the absorption of

electromagnetic radiation in the frequency range 4000-400  $\text{cm}^{-1}$ . With the help of FT-IR analysis, the impact of biofield treatment on bond strength, rigidity and stability of BHT compound can be analysed [28].

### UV-Vis spectroscopic analysis

For UV-Vis spectroscopic analysis, the treated sample was divided into two groups, served as T1 and T2. The UV-Vis spectral analysis was measured using Shimadzu UV-2400 PC series spectrophotometer. The spectrum was recorded with 1 cm quartz cell having a slit width of 2.0 nm over a wavelength range of 200-400 nm. With UV-Vis spectroscopy, it is possible to investigate electron transfers between orbitals or bands of atoms, ions and molecules from the ground state to the first excited state [29].

## Results and Discussion

### X-ray diffraction (XRD)

The X-ray powder diffractograms of control and treated samples showing Bragg angle ( $2\theta$ ) on x-axis and intensity of the peaks on y-axis are presented in Figure 2. The XRD diffractograms showed a series of sharp peaks in the regions of  $10^\circ < 2\theta < 40^\circ$ , which depicted that both samples had high crystallinity and long range order of molecules. The sharp peaks on the diffractograms of the control and treated sample confirm the crystalline nature of BHT [30]. The XRD pattern indicated the orthorhombic crystal structure in the control and treated BHT samples. The crystal structure parameters were computed using PowderX software such as lattice parameter, unit cell volume, density, and molecular weight. The results are presented in Table 1. The data showed that in the control sample, the lattice parameters were found as  $a=15.46$ ,  $b=10.37$ , and  $c=8.93$  Å. While, in treated sample, the lattice parameters were found as  $a=15.59$ ,  $b=10.56$  and  $c=8.71$  Å. It showed that the lattice parameters 'a' and 'b' were increased by 0.84% and

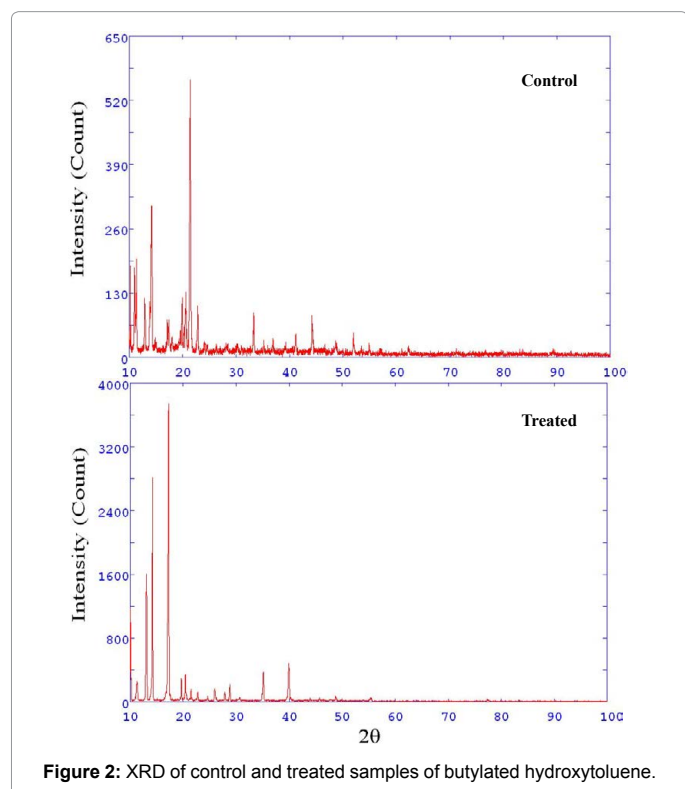


Figure 2: XRD of control and treated samples of butylated hydroxytoluene.

Parameter	Control	Treated	Percent change
Lattice parameter			
a (Å)	15.46	15.59	0.84
b (Å)	10.37	10.56	1.83
c (Å)	8.93	8.71	-2.46
Unit cell volume ( $\times 10^{-23}$ $\text{cm}^3$ )	143.208	143.330	0.090
Density ( $\text{w}/\text{cm}^3$ )	1.029	1.028	-0.10
Molecular weight (g/mol)	222.752	222.941	0.08
Crystallite size (nm)	70.16	59.77	-14.81

Table 1: X-ray diffraction analysis of control and treated butylated hydroxytoluene.

1.83%, respectively. However, the lattice parameter 'c' was decreased by 2.46% in the treated sample as compared to the control. Similarly, the unit cell volume and molecular weight was slightly increased by 0.09% and 0.08%, respectively; whereas, density was decreased by 0.10% in the treated sample as compared to the control. The increase in unit cell volume and change in lattice parameters indicated the presence of internal strain in the treated BHT powder. Besides, the crystallite size computed using Scherrer formula was found as 70.16 nm in control and it was reduced to 59.77 nm in the treated BHT sample. It suggested that crystallite size of the treated sample was significantly reduced by 14.81% as compared to the control. It is reported that the energy produced by mechanical milling had reduced the crystallite size and induced lattice strain in the crystal structure [31]. Thus, it is assumed that biofield energy treatment might induce the energy milling in BHT sample, and that might be responsible for a decrease in crystallite size of treated sample. Recently, our group reported that biofield treatment had reduced the crystallite size in magnesium powder [19]. Moreover, it was reported that crystallite size and surface area are inversely related to each other [32]. The BHT had a poor solubility profile in water that limits its application in pharmaceutical preparations [7]. Hence, the decreased crystallite size of treated BHT might result in increased surface area, and that can play an important role in improving solubility. Therefore, the treated BHT sample may be used in food and pharmaceutical industry with improved solubility profile.

### DSC analysis

This technique is based on the principle that as the BHT sample undergoes any phase transition (e.g. solid to liquid); the alteration was observed in the amount of heat flowing to the sample as compared to the reference. The thermograms for control and treated sample of BHT are presented in Figure 3 that showed the phase transition temperature and the amount of heat involved in that process. The control sample exhibited a sharp endothermic peak at  $71.6^\circ\text{C}$ , whereas the treated sample showed a sharp peak at  $72.25^\circ\text{C}$ . The peaks are due to melting of control and treated samples, and the sharpness of peaks confirms the crystalline nature of BHT sample. The result suggests a slight change in melting temperature of treated sample as compared to the control. The thermograms also showed that the latent heat of fusion ( $\Delta H$ ) was increased from 75.94 J/g (control) to 96.23 J/g in treated BHT sample. It indicated that  $\Delta H$  was significantly increased by 26.72% in the treated sample as compared to the control. It is presumed that biofield energy might increase the potential energy stored in the molecules of treated BHT sample. Hence, the treated sample needs more energy in the form of  $\Delta H$  to undergo the process of melting. Previously, our group reported that biofield treatment has altered the latent heat of fusion in indole, thymol and menthol compounds [17,33].

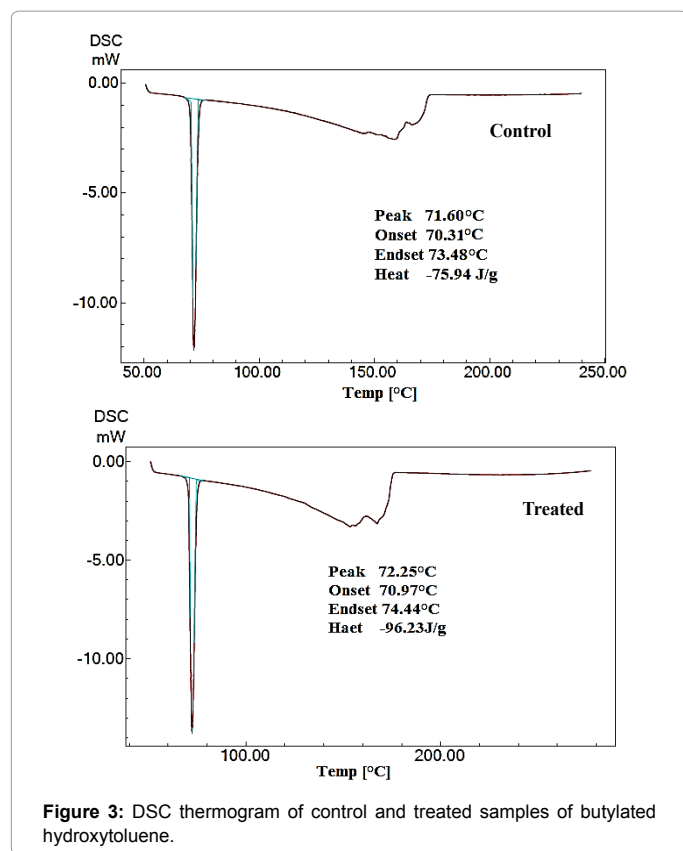


Figure 3: DSC thermogram of control and treated samples of butylated hydroxytoluene.

### TGA/DTG analysis

The TGA thermograms (Figure 4) of the control and treated samples of BHT showed single step decomposition within the temperature range of 100-200°C. From these thermograms, the information related to degradation temperature and the weight of sample lost in that event was collected. The control sample started to decompose around 130°C (onset) and completed around 175°C (end set). However, the treated sample started losing weight around 136°C (onset) and terminated at 185°C (end set). It indicated that onset temperature of decomposition was increased in the treated sample as compared to the control. Besides, DTG thermogram data showed that  $T_{max}$  was found at 152.39°C in the control sample, whereas, it was increased to 158.42°C in the treated BHT sample. It indicated that  $T_{max}$  was also increased in treated sample as compared to the control. Furthermore, the increase in onset temperature of decomposition and  $T_{max}$  in the treated sample of BHT with respect to the control sample may be correlated with the increase in thermal stability of the treated sample after biofield treatment. The data was also supported by DSC studies, which revealed that  $\Delta H$  of treated BHT sample increased as compared to the control sample. As BHT is reported to decompose at higher temperature due to which it offers very less protection to food ingredients. Moreover, BHT is considered as a flammable material and increase in thermal stability may be related to the decreased flammability of compound [13,34]. Hence, it was presumed that the biofield energy treatment might enhance the thermal stability of the treated BHT sample. The increase in thermal stability may enhance its effectiveness in food ingredients at high temperature as well as might assure its safe handling by decreasing the flammability as compared to the control sample.

### FT-IR spectroscopic analysis

Infrared (IR) spectroscopy is based on the vibrations of the atoms in a molecule. The FT-IR spectra of control and treated (T1 and T2) samples of BHT are shown in Figure 5 that has the wavenumber (frequency) of IR rays on the horizontal axis and percent transmittance on the vertical axis. The comparative values of IR peaks of the control sample with treated (T1 and T2) samples are given in Table 2. The major vibration peaks observed were as follows:

**O-H vibrations:** The O-H vibrations are sensitive to hydrogen bonding; however the OH group present in the structure of BHT did not show intermolecular hydrogen bonding due to steric shielding of tert-butyl groups present in the structure. The non-bonded hydroxyl groups in phenols showed absorption in 3700-3584  $\text{cm}^{-1}$  region [35]. In the present study, the strong band observed at 3628  $\text{cm}^{-1}$  in control and T2 sample and 3626  $\text{cm}^{-1}$  in T1 sample was assigned to OH stretching mode of vibration. The strong band observed at 1151  $\text{cm}^{-1}$  in all three samples (control, T1, and T2) was assigned to OH in-plane bending vibration.

**Aromatic C-H vibrations:** The aromatic CH stretching vibration was observed as a weak band at 3068  $\text{cm}^{-1}$  in control and T2 sample whereas at 3150  $\text{cm}^{-1}$  in T2 sample. The in-plane CH bending vibrations was observed at 1230  $\text{cm}^{-1}$  in all three samples (control, T1 and T2).

**Methyl group vibrations:** In the present study, the  $\text{CH}_3$  asymmetric vibration was observed at 2956  $\text{cm}^{-1}$  in the control sample and 2955  $\text{cm}^{-1}$  in both treated samples (T1 and T2). The  $\text{CH}_3$  symmetric stretching mode was observed at 2872  $\text{cm}^{-1}$  in all three samples i.e. control, T1, and T2. Similarly, the bands observed at 1481 and 1431  $\text{cm}^{-1}$  in control and T1 and 1481 and 1433  $\text{cm}^{-1}$  in T2 were assigned to the  $\text{CH}_3$  bending vibrations. The  $\text{CH}_3$  rocking vibration was observed at 1026  $\text{cm}^{-1}$  in all three samples (control, T1 and T2).

**Tert-butyl group vibrations:** In the FT-IR spectra, the strong, sharp bands observed at 1361 and 1396  $\text{cm}^{-1}$  in the control sample and 1363 and 1396  $\text{cm}^{-1}$  in treated samples (T1 and T2) were assigned to tert-butyl bending vibrations.

**C-O vibrations:** In the present study, the FT-IR band observed at 1213  $\text{cm}^{-1}$  in control and T1 sample and 1215  $\text{cm}^{-1}$  in T2 sample was

S. No.	Functional group	Wavenumber ( $\text{cm}^{-1}$ )		
		Control	T1	T2
1.	O-H stretching	3628	3626	3628
2.	C-H stretching (aromatic)	3068	3150	3068
3.	C-H <sub>3</sub> asymmetric stretching	2956	2955	2955
4.	C-H <sub>3</sub> symmetric stretching	2872	2872	2872
5.	C=C stretching (aromatic)	1603	1575	1602
6.	C-H <sub>3</sub> bending	1481 1431	1481 1431	1481 1431
7.	Tert-butyl group	1396 1361	1396 1363	1396 1363
8.	C-H bending (in plane)	1230	1230	1230
9.	C-O stretching (C-OH)	1213	1213	1215
10.	O-H bending (in plane)	1151	1151	1151
11.	C-H <sub>3</sub> rocking	1026	1026	1026
12.	C-C ring stretching	866 769	866 769	866 769
13.	Aromatic ring bending (out of plane)	580	580	580

T1 and T2 are treated samples

Table 2: Vibration modes observed in butylated hydroxytoluene.

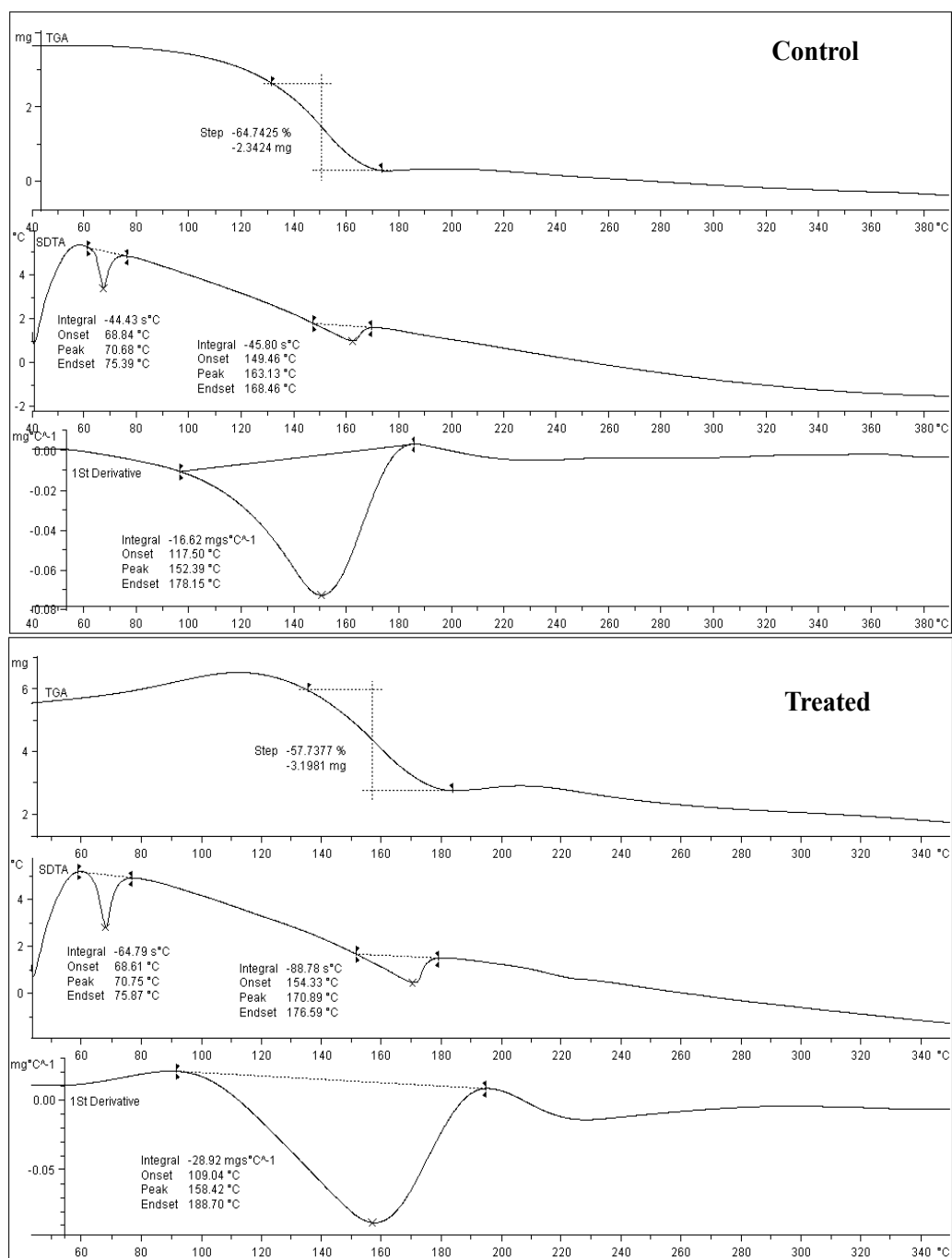


Figure 4: TG/DTG thermograms of control and treated samples of butylated hydroxytoluene.

assigned to C-O stretching mode of C-OH vibration.

**C=C vibrations:** The ring stretching vibration was observed at  $1603\text{ cm}^{-1}$  in control sample, whereas at  $1575$  and  $1602\text{ cm}^{-1}$  in T1 and T2 samples, respectively. The bands observed at  $769$  and  $866\text{ cm}^{-1}$  were assigned to C-C ring stretching mode. Moreover, the band at  $580\text{ cm}^{-1}$  was assigned to ring out-of-plane bending mode in all three samples (control, T1, and T2).

The FT-IR spectrum of the control sample of BHT was well

supported by literature [35,36]. The FT-IR spectra of treated BHT samples (T1 and T2) showed the similar pattern of IR absorption peaks as control sample except C-H aromatic stretching peak and C=C aromatic stretching peak in T1 sample. The C-H aromatic stretching peak was shifted to higher frequency ( $3068 \rightarrow 3150\text{ cm}^{-1}$ ); whereas, C=C aromatic stretching peak was shifted to lower frequency ( $1603 \rightarrow 1575\text{ cm}^{-1}$ ) as compared to the control sample. When a molecule absorbs infrared radiation, its chemical bonds vibrate due to which they can stretch, contract or bend. It was already reported that the peak frequency

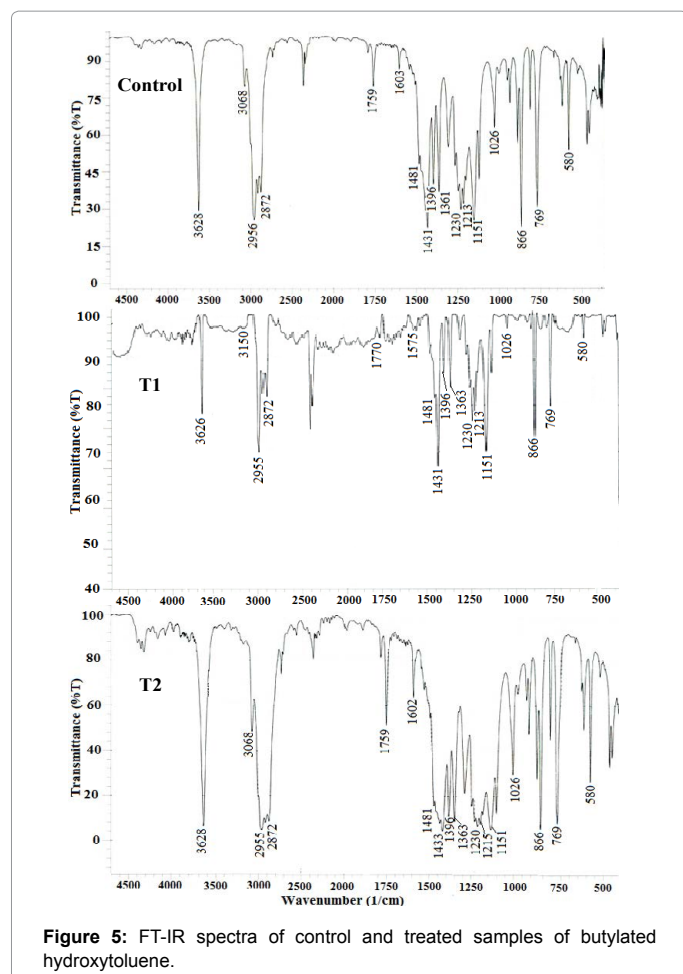


Figure 5: FT-IR spectra of control and treated samples of butylated hydroxytoluene.

( $\nu$ ) in IR spectra for any bond is directly proportional to its bond force constant ( $k$ ). Also, the bond force constant ( $k$ ) is inversely related to average bond length ( $r$ ) [16]. Hence, it is presumed that shifting of peak wavenumber corresponding to aromatic C-H stretching and C=C stretching decreases the bond length of C-H bond and increases the bond length of aromatic C=C bond, respectively. It might occur due to increase in conjugation effect in aromatic ring structure after biofield treatment. As it was evident that conjugation effect increases the stability of structure hence, it could further be correlated to improved stability and decreased flammability of BHT sample after biofield energy treatment [37].

### UV-Vis spectroscopic analysis

The UV spectra of control and treated samples (T1 and T2) of BHT having wavelength of UV-vis light on the horizontal axis and absorbance on the vertical axis are shown in Figure 6. The UV spectrum of control sample showed absorption peaks at  $\lambda_{\text{max}}$  equal to 205, 247, and 278 nm. However the biofield treated sample T1 showed absorption peaks at 204, 223, and 278 nm and T2 showed peaks at 204, 223, and 277 nm. The peak at 247 nm in control sample was shifted to 223 nm in the treated samples. The absorbance is the measurement for amount of the light absorbed and it means that the corresponding wavelength of light on horizontal axis was being absorbed by the BHT sample. The absorption peak is described by one electron excitation from the highest occupied molecular orbital (HOMO) to the lowest occupied molecular orbital (LUMO). LUMO represents the ability to

accept an electron, whereas HOMO represents the ability to donate an electron. In BHT, the HOMO is located over the OH and CH<sub>3</sub> groups, and the HOMO→LUMO transition corresponds to the transfer of electron density from OH and CH<sub>3</sub> groups to the ring [35]. Hence, it is hypothesised that biofield energy treatment might affect this HOMO→LUMO transition due to which the peak at  $\lambda_{\text{max}}$  247 nm was shifted to 223 nm in the treated sample. The result was also supported by FT-IR data that showed the impact of biofield energy treatment possibly on the C=C and C-H stretching of the aromatic ring.

### Conclusions

The results showed the impact of biofield treatment on the lattice parameter, unit cell volume and molecular weight of treated sample. The crystallite size of treated BHT was reduced by 14.8% suggesting the presence of internal strain that could be due to the biofield energy treatment. The DSC analysis showed 26.7% increase in  $\Delta H$ , which revealed that biofield energy probably enhanced the potential energy in treated BHT sample as compared to the control. The TGA/DTG results suggested that thermal stability of treated sample was increased which might help to enhance its effectiveness in food materials and reduce the flammability as compared to the control. The FT-IR analysis revealed the changes in the wavenumber of aromatic C-H bond and C=C bond that suggest the increase in conjugation effect in the benzene ring that probably occurred due to biofield energy treatment. Moreover, the UV-Vis spectra also showed the shifting of peak corresponding to 247 nm towards lower wavelength i.e. 223 nm. Hence, the overall study reported the impact of Mr. Trivedi's biofield energy treatment on the physical, thermal and spectral properties of BHT sample. The altered properties of treated sample could make it more useful in food and pharmaceutical industries by enhancing the solubility and thermal stability along with reduction in the flammability.

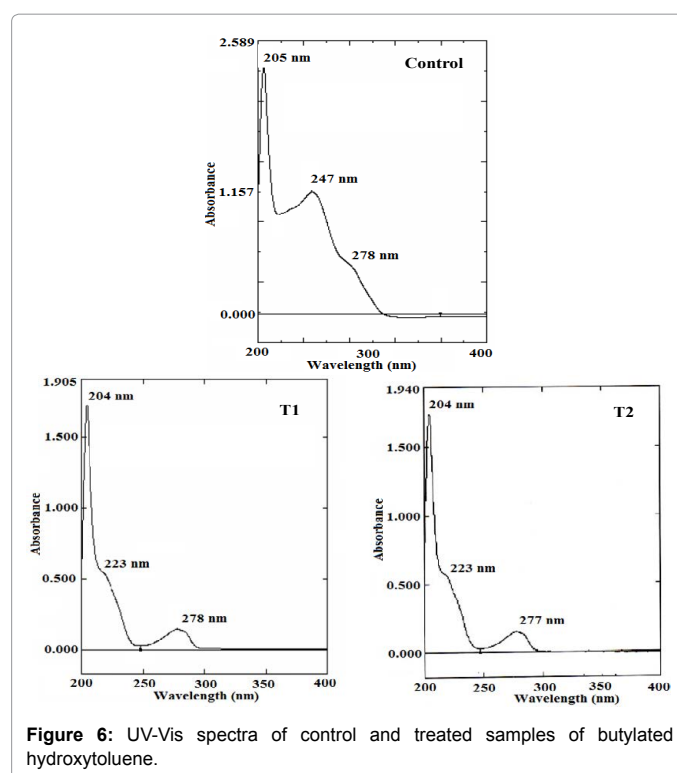


Figure 6: UV-Vis spectra of control and treated samples of butylated hydroxytoluene.

## Acknowledgements

Authors are very grateful for the support of Trivedi Science, Trivedi Master Wellness and Trivedi Testimonials in this research work. The authors would also like to acknowledge the whole team from the Sophisticated Analytical Instrument Facility (SAIF), Nagpur and MGV Pharmacy College, Nashik for providing the instrumental facility.

## References

1. Arouma OI (2003) Methodological considerations for characterizing potential antioxidant actions of bioactive components in plant foods. *Mutat Res* 523-524: 9-20.
2. Pham-Huy LA, He H, Pham-Huy C (2008) Free radicals, antioxidants in disease and health. *Int J Biomed Sci* 4: 89-96.
3. Mattson MP (2000) Apoptosis in neurodegenerative disorders. *Nat Rev Mol Cell Biol* 1: 120-129.
4. Celestino MT, Magalhaes UDO, Fraga AGM, do Carmo FA, Lione V, et al. (2012) Rational use of antioxidants in solid oral pharmaceutical preparations. *Braz J Pharm Sci* 48: 405-415.
5. Troy DB, Beringer P (2006) *Pharmaceuticals stability*. Remington: The science and practice of pharmacy. (21st edn), Lippincott Williams and Wilkins, USA.
6. Aulton ME, Taylor K (2013) *Pharmaceutical preformulation*. Aulton's pharmaceuticals: The design and manufacture of medicines. (4th edn), Elsevier Health Sciences, Edinburgh.
7. Babich H (1982) Butylated hydroxytoluene (BHT): A review. *Environ Res* 29: 1-29.
8. Lobo V, Patil A, Phatak A, Chandra N (2010) Free radicals, antioxidants and functional foods: Impact on human health. *Pharmacogn Rev* 4: 118-126.
9. Bitar A, Ghaddar T, Malek A, Haddad T, Toufeili I (2008) Sensory thresholds of selected phenolic constituents from thyme and their antioxidant potential in sunflower oil. *J Am Oil Chem Soc* 85: 641-646.
10. Akkbi M, Assim ZB, Ahmad FB (2011) Optimization and validation of RP-HPLC-UV/Vis method for determination phenolic compounds in several personal care products. *Int J Anal Chem* 2011: 1-9.
11. Sanhueza J, Nieto S, Valenzuela A (2000) Thermal stability of some commercial synthetic antioxidants. *J Am Oil Chem Soc* 77: 933-936.
12. Roos YH (2003) Thermal analysis, state transitions and food quality. *J Therm Anal Calorim* 71: 197-203.
13. Lewis RA (1998) *Lewis' dictionary of toxicology*. CRC Press.
14. Akers MJ (1982) Antioxidants in pharmaceutical products. *J Parenter Sci Technol* 36: 222-228.
15. Reda SY (2011) Evaluation of antioxidants stability by thermal analysis and its protective effect in heated edible vegetable oil. *Cienc Tecnol Aliment* 31: 475-480.
16. Trivedi MK, Patil S, Shettigar H, Singh R, Jana S (2015) An impact of biofield treatment on spectroscopic characterization of pharmaceutical compounds. *Mod Chem appl* 3: 159.
17. Trivedi MK, Patil S, Mishra RK, Jana S (2015) Structural and physical properties of biofield treated thymol and menthol. *J Mol Pharm Org Process Res* 3: 127.
18. Trivedi MK, Nayak G, Patil S, Tallapragada RM, Latiyal O, et al. (2015) An evaluation of biofield treatment on thermal, physical and structural properties of cadmium powder. *J Thermodyn Catal* 6: 147.
19. Trivedi MK, Tallapragada RM, Branton A, Trivedi D, Nayak G, et al. (2015) Potential impact of biofield treatment on atomic and physical characteristics of magnesium. *Vitam Miner* 3: 129.
20. Uchida S, Iha T, Yamaoka K, Nitta K, Sugano H (2012) Effect of biofield therapy in the human brain. *J Altern Complement Med* 18: 875-879.
21. NIH [2008] National Center for Complementary and Alternative Medicine. CAM Basics. Publication 347.
22. Rubik B (2002) The biofield hypothesis: Its biophysical basis and role in medicine. *J Altern Complement Med* 8: 703-717.
23. Suzuki K, Uchida S, Kimura T (2009) Safety and efficacy of biofield therapy in Japan. *Soc Integr Med* 2: 37-43.
24. Shinde V, Sances F, Patil S, Spence A (2012) Impact of biofield treatment on growth and yield of lettuce and tomato. *Aust J Basic Appl Sci* 6: 100-105.
25. Sances F, Flora E, Patil S, Spence A, Shinde V (2013) Impact of biofield treatment on ginseng and organic blueberry yield. *Agrivita J Agric Sci* 35: 22-29.
26. Trivedi MK, Patil S, Shettigar H, Bairwa K, Jana S (2015) Phenotypic and biotypic characterization of *Klebsiella oxytoca*: An impact of biofield treatment. *J Microb Biochem Technol* 7: 203-206.
27. Trivedi MK, Patil S, Shettigar H, Gangwar M, Jana S (2015) An effect of biofield treatment on multidrug-resistant *Burkholderia cepacia*: A multihost pathogen. *J Trop Dis* 3: 167.
28. Coates J (2000) Interpretation of infrared spectra, a practical approach. *Encyclopedia of analytical chemistry*. John Wiley and Sons Ltd., Chichester.
29. Hunger M, Weitkamp J (2001) In situ IR, NMR, EPR, and UV/Vis spectroscopy: Tools for new insight into the mechanisms of heterogeneous catalysis. *Angew Chem Int Ed Engl* 40: 2954-2971.
30. Rudrangi SR, Bhomia R, Trivedi V, Vine GJ, Mitchell JC, et al. (2015) Influence of the preparation method on the physicochemical properties of indomethacin and methyl- $\beta$ -cyclodextrin complexes. *Int J Pharm* 479: 381-390.
31. Fuse M, Shirakawa Y, Shimosaka A, Hidaka J (2003) Mechanically strain-induced modification of selenium powders in the amorphization process. *J Nanopart Res* 5: 97-102.
32. Behnajady MA, Aalamdari ME, Modirshahla N (2013) Investigation of the effect of heat treatment process on characteristics and photocatalytic activity of TiO<sub>2</sub>-UV100 nanoparticles. *Environ Prot Eng* 39: 33-46.
33. Trivedi MK, Tallapragada RM, Branton A, Trivedi D, Nayak G, et al. (2015) Biofield treatment: A potential strategy for modification of physical and thermal properties of indole. *J Environ Anal Chem* 2: 152.
34. Rybinski P, Janowska G, Jozwiak M, Pajak A (2012) Thermal stability and flammability of butadiene-styrene rubber nanocomposites. *Therm Anal Calorim* 109: 561-571.
35. Babu PC, Sundaraganesan N, Dereli O, Turkan E (2011) FT-IR, FT-Raman spectra, density functional computations of the vibrational spectra and molecular geometry of butylated hydroxy toluene. *Spectrochim Acta A Mol Biomol Spectrosc* 79: 562-569.
36. Ammawath W, Man YBC, Rahman RBA, Baharin BS (2006) A fourier transform infrared spectroscopic method for determining butylated hydroxytoluene in palm olein and palm oil. *J Am Oil Chem Soc* 83: 187-189.
37. Backus JK, Bernard DL, Darr WC, Saunders JH (1968) Flammability and thermal stability of isocyanate-based polymers. *J Appl Polym Sci* 12: 1053-1074.